Original Article

Diagnostic value of shear wave elastography quantification combined with conventional ultrasound in salivary gland tumors

Qian Yu, Angang Ding, Qianqian Chen, Jiaxin Zuo, Jinye Cao, Ping Xiong

Department of Ultrasound, Ninth People's Hospital, Shanghai Jiaotong University School of Medicine, Shanghai, China

Contributions: (I) Conception and design: P Xiong, Q Yu; (II) Administrative support: P Xiong; (III) Provision of study materials or patients: Q Yu, A Ding, Q Chen; (IV) Collection and assembly of data: Q Yu, A Ding, J Zuo; (V) Data analysis and interpretation: Q Yu, J Zuo, J Cao; (VI) Manuscript writing: All authors; (VII) Final approval of manuscript: All authors.

Correspondence to: Ping Xiong, MD, PhD. Department of Ultrasound, Ninth People's Hospital, Shanghai Jiaotong University School of Medicine, 639 Zhizaoju Road, Huangpu, Shanghai 200011, China. Email: xiongpxp@163.com.

Background: The histopathological classification of salivary gland tumors is extremely complex. The imaging manifestations of some tumors are nonspecific. It is particularly important to improve the value of ultrasound in the diagnosis of salivary gland tumors. This study aimed to analyze the diagnostic value of different parameters of shear wave elastography (SWE) in the quantitative diagnosis of salivary gland tumors, and to evaluate the value of SWE combined with conventional ultrasound.

Methods: The study was conducted retrospectively. Patients who underwent salivary gland tumor resection from April 2021 to November 2022 in the Ninth People's Hospital, Shanghai Jiaotong University School of Medicine were randomly recruited to the study. A total of 305 masses were divided into an elastography group (150 cases) and a control group (155 cases). The control group underwent conventional ultrasonography, whereas the elastography group underwent conventional ultrasonography and elastography. The Young's modulus E of the mass was quantitatively measured in the elastography group, including maximum cross-sectional area (S), maximum Young's modulus (Emax), mean Young's modulus (Emean), and Young's modulus standard deviation (SD). Pathologic diagnosis was used as the reference standard to determine the cut-off of shear wave elastography of salivary gland tumors, and the diagnostic performance of the 2 groups was compared.

Results: In the elastography group, the diagnostic value of Emax·S (the product of the maximum Young's modulus of the mass and the maximum cross-sectional area of the mass) in the differential diagnosis of malignant tumors (MT) and non-malignant tumors (NMT) was the highest, with a sensitivity and specificity of 72.0% and 80.0%, respectively. The diagnostic value of Emax/D (the quotient of the maximum Young's modulus of the mass and the maximum diameter of the mass) in the differential diagnosis of pleomorphic adenoma (PA) and adenolymphoma (AL) was the highest, with a sensitivity and specificity of 62.3% and 82.4%, respectively. The receiver operating characteristic (ROC) curves for the diagnosis of salivary gland tumors were compared between the elastography group and the control group. The area under the curve (AUC) of the elastography group was 0.915, the sensitivity, specificity, and Youden index were 84.0%, 88.0%, and 0.720, respectively. The AUC of the control group was 0.906, the sensitivity, specificity, and Youden index were 76.0%, 90.0%, and 0.660, respectively, which is the main finding of the study.

Conclusions: SWE can be used as a complementary method for the diagnosis of salivary gland tumors, which has certain value in improving the diagnostic performance. As a result, the sensitivity is improved but the specificity is worsened by addition of SWE to B-mode ultrasound and color Doppler flow imaging (CDFI).

Keywords: Salivary gland tumor; shear wave elastography; ultrasonography; diagnostic value

Submitted Jan 27, 2023. Accepted for publication Jul 20, 2023. Published online Aug 14, 2023.
doi: 10.21037/qims-23-103
View this article at: https://dx.doi.org/10.21037/qims-23-103

Introduction

Salivary gland tumors are a relatively rare type of head and neck tumor (1). Surgery is an important and effective treatment for salivary gland tumors, but there are great differences in surgical methods for different types of tumors (2). Inappropriate surgery may cause postoperative complications such as facial paralysis and recurrence (3). Therefore, differentiating salivary gland lesions becomes an important part of preoperative treatment planning (4). Fine needle aspiration cytology (FNAC) is still considered the most authoritative tool in clinical practice (5). The histopathological classification of salivary gland tumors is extremely complex, and the imaging manifestations of some tumors are nonspecific (6). In recent years, ultrasound has become the first-line imaging method for salivary gland lesions (7), and the application of new ultrasound technologies such as contrast-enhanced ultrasound, strain-elastic ultrasound, and shear wave elastography (SWE) has received attention (8).

Different human tissues have different degrees of elasticity due to the properties of the extracellular matrix (9). The change of tissue hardness may be related to the occurrence of various diseases. At present, ultrasonic techniques that can quantitatively measure tissue hardness include virtual touch tissue imaging (VTIQ) and SWE. They both are non-invasive technologies that can quantitatively evaluate the elasticity of the mass by measuring average shear wave velocity (SWV) of a region of interest (ROI) in the mass (10,11). SWE can convert SWV into Young's modulus, and the stiffness of the mass is expressed in Kpa. The technique was first used to measure the hardness of liver tissue to assess the degree of fibrosis in the liver (12), which has been considered an effective method for the evaluation of thyroid, breast, and liver lesions (13,14). The results of SWE in the differential diagnosis of benign and malignant salivary gland tumors vary greatly as single ultrasound elastography has limited value in the differential diagnosis of salivary gland tumors (15-17). We conducted this study to clarify the value of SWE. This study evaluated the diagnostic value of SWE combined with B-mode ultrasound and color Doppler flow imaging (CDFI), which was used to quantitatively diagnose the benign and malignant salivary gland tumors. We present this article in accordance with the STARD reporting checklist (available at https://qims.amegroups.com/article/view/10.21037/qims-23-103/rc).

Methods

Patients

The study was conducted in accordance with the Declaration of Helsinki (as revised in 2013) and with the approval of the Ethics Committee of the Ninth People's Hospital, Shanghai Jiaotong University School of Medicine. The requirement for individual consent in this retrospective analysis was waived. The age, gender, and other general characteristics of the study population and ultrasound image information of the patients were collected.

We randomly selected patients who were admitted to the Ninth People's Hospital, Shanghai Jiaotong University School of Medicine for salivary gland tumor resection from April 2021 to November 2022. Patients were eligible for the study if they met the following inclusion criteria: (I) preoperative ultrasound showed salivary gland mass; (II) no treatment, including surgery, radiotherapy, or chemotherapy, had been performed before ultrasound examination; (III) definite pathological diagnosis after operation. In contrast, patients were excluded if they met any of the following exclusion criteria: (I) poor ultrasound image quality; (II) controversial pathological diagnosis; (III) a depth of the mass of greater than 3 cm, which would affect the imaging quality, and the data needed to be discarded.

According to the method of ultrasound examination, the patients were divided into an elastography group (150 cases) and a control group (155 cases). The control group underwent B-mode ultrasound and CDFI; the elastography group underwent B-mode ultrasound, CDFI, and SWE. Postoperative pathological diagnosis was used as the reference standard for diagnosis. Both the assessors of the reference standard and the performers of the test were blinded to the result. Salivary gland tumors were classified according to the World Health Organization (WHO) 5th edition of Classification of Pathology and Genetics of Head and Neck Tumors published in 2022 (6).

Ultrasound examination procedure

Ultrasound was performed using an Aixplorer ultrasound diagnostic equipment (Supersonic Imaging Co., Aix-en-Provence, France), as well as an SL15-4 linear array probe (frequency 4–15 MHz). During the examination, pressure on the mass was avoided. Ultrasound gel could be thickly applied to the skin to increase the buffer, which was implemented in all cases in this study.

In B-mode ultrasound, the location, margin, shape, echogenicity, architecture, posterior acoustic effect, and maximum diameter (D) of the salivary gland mass were collected. In CDFI, the blood flow of salivary gland mass was divided into 4 grades according to the distribution of blood flow: (I) Grade 0 was no blood flow signal in the mass, (II) Grade 1 was small blood flow signal, with 1–2 punctate blood flow signals seen in the mass, (III) Grade 2 was moderate blood flow, with 3–4 punctate blood flow signals or a blood vessel with a clear wall seen in the mass, (IV) Grade 3 was rich blood flow, more than 4 punctate blood flow signals or 2 blood vessels with a clear wall in the mass. In SWE, the sampling frame was placed on the maximum cross section of the mass, containing part of the surrounding glandular tissue. When the sampling frame was filled and stable, an ROI was drawn according to the boundary of the mass, and the Young's modulus E of the mass was quantitatively measured, including maximum cross-sectional area (S), maximum Young's modulus (Emax), mean Young's modulus (Emean), and Young's modulus standard deviation (SD). The Q-box was set as 2 mm in size and placed in the hardest area of the mass and the surrounding normal glandular tissue. The ratio of Young's modulus (Eratio) of the 2 were quantitatively measured. A total of 3 elastic images were acquired at the same location, and average figures were calculated.

Statistical analysis

The software SPSS 26.0 (IBM Corp., Armonk, NY, USA) was used for statistical analysis. Count data were expressed as frequency, and chi-square test/Fisher's exact test was used for comparison between groups. The measurement data were tested for normality and homogeneity of variance by Kolmogorov-Smirnov test and Levene's test and were expressed as mean ± standard deviation (SD). The differences between groups were analyzed by independent sample *t*-test or one-way analysis of variance (ANOVA). Ordinal data were analyzed using the nonparametric rank sum test. The receiver operating characteristic (ROC) curves of different modes were compared between the elastography group and the control group, and the diagnostic value was analyzed. All P values were 2-sided, with a test level of α=0.05, and P<0.05 was considered statistically significant.

Results

Finally, 305 cases of mass were included, including 150 in the elastography group and 155 in the control group. In the elastography group, there were 109 benign tumors, 25 malignant tumors (MT), 2 benign soft tissue tumors, 5 lymphatic and hematopoietic system tumors, 3 non-neoplastic epithelial lesions, and 6 others (including 4 cases of lymphoid hyperplasia and 2 cases of inflammatory lesions). Among them, pleomorphic adenoma (PA) and adenolymphoma (AL) were the most common benign tumors, followed by basal cell adenoma. Their numbers were 61, 34, and 14, respectively. Malignant PA and adenoid cystic carcinoma were the most common MT, followed by mucoepidermoid carcinoma. Their numbers were 7, 6, and 4, respectively. In the control group, there were 114 benign tumors, 25 MT, 2 benign soft tissue tumors, 6 lymphatic and hematopoietic system tumors, 1 non-neoplastic epithelial lesion, and 7 others (including 6 cases of lymphoid hyperplasia and 1 case of lymph node granulomatous lesions). Among them, PA and AL were the most common benign tumors, followed by basal cell adenoma. Their numbers were 59, 32, and 11, respectively. Lympho-epithelioma was the most common MT, followed by malignant PA and adenoid cystic carcinoma. Their numbers were 6, 4, and 4, respectively. The conventional ultrasound parameters were compared between the 2 groups, which had no significant difference (*Table 1*).

Conventional ultrasound parameters of MT and non-malignant tumors (NMT) in the 2 groups were compared respectively, and the data showed that there were no significant differences in age, gender, and D of the mass (P>0.05), whereas there were statistical differences in margin, shape, architecture, posterior acoustic effect, and CDFI (P<0.05) (*Table 2*). The parameters of MT and NMT in the elastography group were compared. There were significant differences in S (2.9±1.3 *vs.* 2.0±1.8 cm^2), Emax (122.8±75.7 *vs.* 60.5±51.0 KPa), Emean (28.9±18.9 *vs.* 20.2±17.7 KPa), SD (22.6±16.2 *vs.* 10.4±8.9 KPa), and Eratio (8.4±6.3 *vs.* 4.7±3.9) between MT and NMT (P<0.05). There were significant differences in

Table 1 Baseline characteristics of Elastography group and Control group

Characteristics	Elastography group, n=150	Control group, n=155	P value
Age, years	50.6±16.7	49.4±18.4	0.550
Gender, M/F	82/68	61/94	0.008
Pathological classification			0.964
Benign tumors	109	114	
Malignant tumors	25	25	
Benign soft tissue tumors	2	2	
Tumors of the hematopoietic system	5	6	
Non-neoplastic epithelial lesions	3	1	
Others	6	7	
D (cm)	2.1±0.9	2.4±1.1	0.070
Location			0.788
Parotid gland	123	131	
Submandibular gland	23	22	
Sublingual gland	1	0	
Accessory parotid gland	3	2	
Margin			0.052
Defined	34	62	
Still clear	86	57	
Not very clear	17	25	
Ill-defined	13	11	
Shape			0.647
Oval	90	96	
Still regular	6	2	
Not very regular	11	18	
Lobular	25	24	
Irregular	18	15	
Echogenicity			0.162
More hypoechoic	3	5	
Hypoechoic	97	109	
Mixed echo	50	41	
Architecture			0.113
Homogeneous	23	12	
Still even	4	1	
Not very even	38	50	
Heterogeneous	45	40	
Heterogeneous and anechoic	31	36	
Heterogeneous and hyperechoic	9	16	

Table 1 (*continued*)

Table 1 (*continued*)

Characteristics	Elastography group, n=150	Control group, n=155	P value
Posterior acoustic effect			0.497
Enhanced	116	124	
Slightly enhanced	12	14	
No distinguishable change	18	15	
Attenuation	4	2	
CDFI			0.070
0	16	10	
1	44	68	
2	27	33	
3	63	44	

Data are presented as mean ± standard deviation. M, male; F, female; D, maximum diameter; CDFI, color Doppler flow imaging.

Table 2 Distribution of conventional ultrasound characteristics of MT and NMT in elastography group and control group

Characteristics	Elastography group, n=150			Control group, n=155		
	MT, n=25	NMT, n=125	P value	MT, n=25	NMT, n=130	P value
Age, years	47.6±16.2	51.2±16.8	0.322	54.3±16.7	48.4±18.6	0.144
Gender, M/F	13/12	69/56	0.769	9/16	52/78	0.708
D (cm)	2.5±0.7	2.1±1.0	0.063	2.8±1.7	2.3±1.0	0.059
Location			<0.001			0.147
Parotid gland	14	109		19	112	
Submandibular gland	9	14		5	17	
Sublingual gland	1	0		0	0	
Accessory parotid gland	1	2		1	1	
Margin			<0.001			<0.001
Defined	0	34		1	61	
Still clear	10	76		6	51	
Not very clear	5	12		9	16	
Ill-defined	10	3		9	2	
Shape			<0.001			<0.001
Oval	4	86		5	91	
Still regular	0	6		0	2	
Not very regular	1	10		6	12	
Lobular	5	20		2	22	
Irregular	15	3		12	3	

Table 2 (*continued*)

Table 2 (*continued*)

Characteristics	Elastography group, n=150			Control group, n=155		
	MT, n=25	NMT, n=125	P value	MT, n=25	NMT, n=130	P value
Echogenicity			0.135			0.912
More hypoechoic	2	1		1	4	
Hypoechoic	17	80		17	92	
Mixed echo	6	44		1	34	
Architecture			<0.001			0.045
Homogeneous	0	23		0	12	
Still even	0	4		0	1	
Not very even	2	36		5	45	
Heterogeneous	10	35		12	28	
Heterogeneous and anechoic	7	24		1	35	
Heterogeneous and hyperechoic	6	3		7	9	
Posterior acoustic effect			<0.001			<0.001
Enhanced	13	103		11	113	
Slightly enhanced	3	9		6	8	
No distinguishable change	5	13		6	9	
Attenuation	4	0		2	0	
CDFI			0.010			0.014
0	5	11		6	4	
1	10	34		11	57	
2	4	23		3	30	
3	6	57		5	39	

Data are presented as mean ± standard deviation. MT, malignant tumors; NMT, non-malignant tumors; M, male; F, female; D, maximum diameter; CDFI, color Doppler flow imaging.

Emax (74.0±55.9 *vs.* 49.9±46.6 KPa), Emean (25.7±22.8 *vs.* 15.7±7.3 KPa) and SD (12.7±9.7 *vs.* 8.4±7.0 KPa) between PA and AL (P<0.05), whereas there was no statistically significant difference in S and Eratio (P>0.05) (*Table 3*). The corresponding ROC curve of each parameter was drawn and analyzed. It was concluded that the diagnostic value of Emax·S in the differential diagnosis of MT and NMT was the highest, and the cut-off and area under the curve (AUC) was 195.6 KPa·cm² and 0.788, respectively. The sensitivity, specificity, and Youden index based on the above parameter was 72.0%, 80.0%, and 0.520, respectively. In addition, the cut-off of Emax, Emean, SD, and Eratio was 86.3 KPa, 28.3 Kpa, 16.4 KPa, and 8.8, respectively (*Figure 1*, *Table 4*). The diagnostic value of Emax/D in the differential diagnosis of PA and AL was the highest, the cut-off and AUC was 24.2 KPa/cm and 0.779, respectively. The sensitivity, specificity, and Youden index based on the above parameter was 62.3%, 82.4%, and 0.446, respectively. In addition, the cut-off of Emax, Emean, and SD was 40.9 KPa, 17.4 KPa, and 7.0 KPa, respectively (*Figure 1*, *Table 5*).

ROC curve analysis of different ultrasonic imaging modes in the diagnosis of MT between the elastography group and the control group showed that B-mode ultrasound combined with CDFI and SWE in the elastography group had the highest diagnostic value, with an AUC of 0.915. The sensitivity, specificity, and Youden index were 84.0%,

Table 3 Elastic parameters in the elastography group

Parameters	MT, n=25	NMT, n=125	P (MT *vs.* NMT)	PA, n=61	AL, n=34	P (PA *vs.* AL)
D (cm)	2.5±0.7	2.1±1.0	0.063	2.0±0.9	2.6±1.2	0.010
S (cm^2)	2.9±1.3	2.0±1.8	0.018	2.1±2.0	2.5±1.6	0.429
Emax (KPa)	122.8±75.7	60.5±51.0	<0.001	74.0±55.9	49.9±46.6	0.035
Emean (KPa)	28.9±18.9	20.2±17.7	0.028	25.7±22.8	15.7±7.3	0.002
SD (KPa)	22.6±16.2	10.4±8.9	0.001	12.7±9.7	8.4±7.0	0.014
Eratio	8.4±6.3	4.7±3.9	0.010	5.6±4.4	4.1±3.6	0.100
Emax·D (KPa·cm)	334.9±272.7	141.8±125.8	0.002	162.7±155.3	164.0±154.3	0.974
Emax/D (KPa/cm)	47.8±24.4	31.2±24.6	0.003	38.6±25.9	18.8±10.4	<0.001
Emax·S (KPa·cm^2)	398.5±367.6	156.9±146.7	0.004	194.0±184.6	174.1±165.7	0.752
Emax/S (KPa·cm^2)	44.9±25.0	43.7±37.0	0.881	51.2±39.8	25.0±16.6	<0.001
Emean·D (KPa/cm)	77.7±64.6	44.8±43.4	0.022	55.0±48.6	45.8±40.3	0.433
Emean/D (KPa/cm)	11.5±6.9	10.9±9.0	0.759	13.8±10.6	6.7±3.2	<0.001
Emean·S (KPa·cm^2)	89.4±81.6	47.1±40.5	0.012	62.5±56.6	45.6±40.5	0.345
Emean/S (KPa/cm^2)	11.2±7.2	16.2±14.3	0.013	18.6±15.0	9.8±7.3	<0.001

Data are presented as mean ± standard deviation. MT, malignant tumors; NMT, non-malignant tumors; PA, pleomorphic adenoma; AL, adenolymphoma; Emax, maximum Young's modulus; Emean, mean Young's modulus; SD, Young's modulus standard deviation; Eratio, Young's modulus ratio of mass-to-surrounding normal glands; S, maximum cross-sectional area; D, maximum diameter.

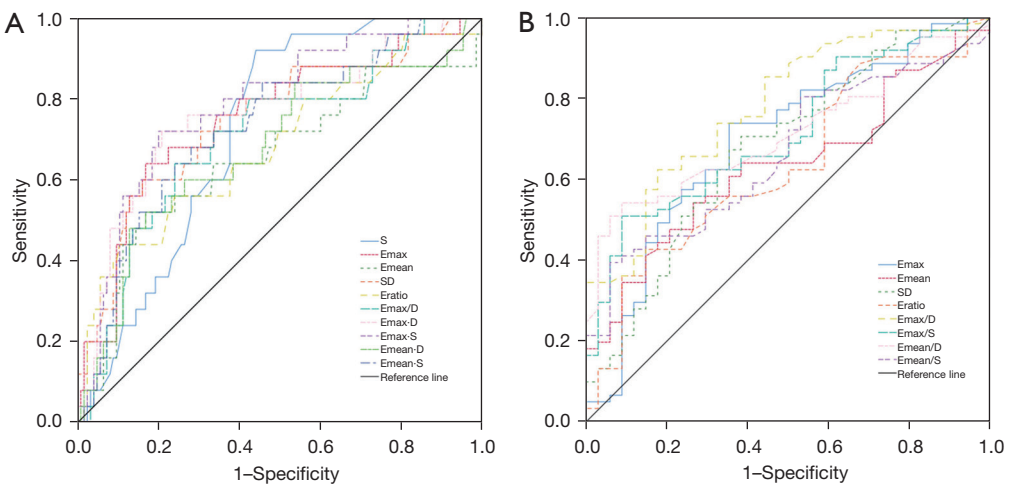

Figure 1 ROC curves of elastic parameters between different masses in Elastography group. (A) ROC curves of elastic parameters between MT and NMT in Elastography group. The diagnostic value of Emax·S in the differential diagnosis of MT and NMT was the highest, and the AUC was 0.788. The sensitivity, specificity and Youden index based on this parameter was 72.0%, 80.0% and 0.520, respectively. (B) ROC curves of elastic parameters between PA and AL in Elastography group. The diagnostic value of Emax/D in the differential diagnosis of PA and AL was the highest, the AUC was 0.779, respectively. The sensitivity, specificity and Youden index based on the above parameter was 62.3%, 82.4% and 0.446, respectively. ROC, receiver operating characteristic; AUC, area under the curve; MT, malignant tumors; NMT, non-malignant tumors; PA, pleomorphic adenoma; AL, adenolymphoma; Emax, maximum Young's modulus; Emean, mean Young's modulus; SD, Young's modulus standard deviation; Eratio, Young's modulus ratio of mass-to-surrounding normal glands; S, maximum cross-sectional area; D, maximum diameter.

Table 4 ROC curves of elastic parameters between MT and NMT in the elastography group

Parameters	Cut-off	AUC (95% CI)	AUC	Sensitivity (%)	Specificity (%)	Youden index
S (cm^2)	1.55	0.724 (0.637, 0.810)	0.724	92.0	56.0	0.480
Emax (KPa)	86.3	0.753 (0.642, 0.864)	0.753	64.0	83.2	0.472
Emean (KPa)	28.3	0.653 (0.520, 0.785)	0.653	52.0	83.2	0.352
SD (KPa)	16.4	0.750 (0.638, 0.862)	0.750	60.0	84.0	0.440
Eratio	8.8	0.683 (0.559, 0.807)	0.683	44.0	89.6	0.336
Emax·D (KPa·cm)	182.6	0.709 (0.651, 0.873)	0.709	72.0	79.2	0.512
Emax/D (KPa/cm)	40.5	0.762 (0.596, 0.822)	0.762	64.0	76.0	0.400
Emax·S (KPa·cm^2)	195.6	0.788 (0.693, 0.883)	0.788	72.0	80.0	0.520
Emean·D (KPa·cm)	61.8	0.679 (0.555, 0.803)	0.679	52.0	83.2	0.352
Emean·S (KPa·cm^2)	46.1	0.733 (0.626, 0.839)	0.733	68.0	72.0	0.400

ROC, receiver operating characteristic; AUC, area under the curve; MT, malignant tumors; NMT, non-malignant tumors; Emax, maximum Young's modulus; Emean, mean Young's modulus; SD, Young's modulus standard deviation; Eratio, Young's modulus ratio of mass-to-surrounding normal glands; S, maximum cross-sectional area; D, maximum diameter.

Table 5 ROC curves of elastic parameters between PA and AL in the elastography group

Parameters	Cut-off	AUC (95% CI)	AUC	Sensitivity (%)	Specificity (%)	Youden index
Emax (KPa)	40.9	0.696 (0.583, 0.808)	0.696	73.8	64.7	0.385
Emean (KPa)	17.4	0.633 (0.522, 0.745)	0.633	54.1	73.5	0.276
SD (KPa)	7.0	0.678 (0.565, 0.792)	0.678	70.5	61.8	0.323
Eratio	5.2	0.634 (0.519, 0.749)	0.634	42.6	85.3	0.279
Emax/D (KPa/cm)	24.2	0.779 (0.685, 0.874)	0.779	62.3	82.4	0.446
Emax/S (KPa/cm^2)	43.3	0.716 (0.613, 0.819)	0.716	50.8	91.2	0.420
Emean/D (KPa/cm)	10.1	0.714 (0.612, 0.815)	0.714	54.1	91.2	0.453
Emean/S (KPa/cm^2)	21.9	0.663 (0.554, 0.772)	0.663	39.3	94.1	0.335

ROC, receiver operating characteristic; AUC, area under the curve; PA, pleomorphic adenoma; AL, adenolymphoma; Emax, maximum Young's modulus; Emean, mean Young's modulus; SD, Young's modulus standard deviation; Eratio, Young's modulus ratio of mass-to-surrounding normal glands; S, maximum cross-sectional area; D, maximum diameter.

88.0%, and 0.720, respectively, and those of B + CDFI were 76.0%, 92.8%, and 0.688, respectively. In the control group, the AUC of B + CDFI was 0.906, and the sensitivity, specificity, and Youden index were 76.0%, 90.0%, and 0.660, respectively (*Figure 2*, *Table 6*).

Discussion

According to the latest WHO classification, salivary gland tumors are divided into 5 categories. In the new classification, some benign tumors, such as lipoma and hemangioma, and some malignant tumors, such as lymphoma, which also occur in other organs, are listed separately. Lymphoma, as a malignant tumor, is treated with chemotherapy, which is different from conventional salivary gland malignancies that are mainly treated with surgery. Malignant tumors require extensive surgical treatment according to oncological principles, often requiring dissection of cervical lymph nodes, whereas benign tumors require minimally invasive surgical treatment (18). We believe that it is important to distinguish MT from all salivary gland masses to better help us formulate treatment

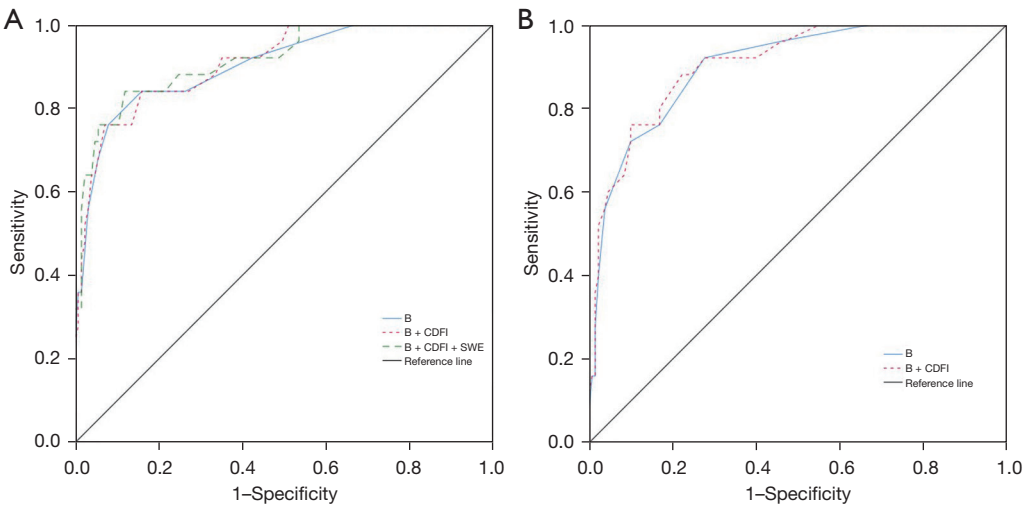

Figure 2 ROC curves of different ultrasound modes in the elastography group and control group for the diagnosis of malignant tumors. (A) ROC curves of different ultrasound modes in the elastography group for the diagnosis of malignant tumors. B + CDFI + SWE had the highest diagnostic value, with an AUC of 0.915. The sensitivity, specificity, and Youden index were 84.0%, 88.0%, and 0.720, respectively. The sensitivity, specificity, and Youden index of B + CDFI were 76.0%, 92.8%, and 0.688, respectively. (B) ROC curves of different ultrasound modes in the control group for the diagnosis of malignant tumors. The AUC of B + CDFI was 0.906, and the sensitivity, specificity, and Youden index were 76.0%, 90.0%, and 0.660, respectively. ROC, receiver operating characteristic; AUC, area under the curve; B, B-mode ultrasound; CDFI, color Doppler flow imaging; SWE, shear wave elastography.

Table 6 ROC curves of different ultrasound modes in the elastography group and the control group

Group	AUC (95% CI)	AUC	Sensitivity (%)	Specificity (%)	Youden index
Group 1 B	0.903 (0.835, 0.971)	0.903	76.0	92.0	0.680
Group 1 B + CDFI	0.908 (0.846, 0.971)	0.908	76.0	92.8	0.688
Group 1 B + CDFI + SWE	0.915 (0.851, 0.978)	0.915	84.0	88.0	0.720
Group 2 B	0.901 (0.840, 0.962)	0.901	92.0	72.3	0.643
Group 2 B + CDFI	0.906 (0.847, 0.964)	0.906	76.0	90.0	0.660

ROC, receiver operator characteristic; AUC, area under the curve; Group 1, elastography group; Group 2, control group; B, B-mode ultrasound; CDFI, color Doppler flow imaging; SWE, shear wave elastography.

plans. Therefore, in this study, we divided the collected salivary gland masses into 2 groups, namely, MT and NMT.

In the selection of elastic imaging parameters, we included the S, Emax, Emean, SD, and Eratio. Eratio can reflect a change of the neoplasm compared with the gland. In the SWE differential diagnosis of breast mass, a similar principle was used to establish mass-to-fat ratio (19). Heřman *et al.*'s study in 2017 (20) also proposed the elastic parameter CSV (the ratio of the maximum and minimum of the Young's modulus), which also showed a significant difference between benign and malignant tumors. The study showed that there were statistically significant differences in the Eratio (8.4±6.3 *vs.* 4.7±3.9) between MT and NMT ($P<0.05$), and the cut-off was 8.8. This indicated that the MT had higher hardness, which was also consistent with our findings on Emax and Emean. In addition, we believe that the hardness of the mass may be related to the size of the mass. We delineated the ROI according to the mass boundary in the largest transverse section of the mass. In our study, the S of MT and NMT was 2.9±1.3 and 2.0±1.8 cm^2, respectively, with significant differences, indicating that malignant tumors are often larger than benign tumors.

This may be related to the fast growth rate of malignant tumors. Malignant tumors often attract patients' attention due to facial masses, and even symptoms such as nerve compression. Benign tumors, on the other hand, tend to be smaller, grow more slowly, are often found accidentally or during routine physical examinations. In data processing, we have computed Emax and Emean with D and S, respectively, and included them into the ROC curves of salivary gland tumors. We found that Emax·S had the highest diagnostic value in the differentiation of MT and NMT, with a sensitivity and specificity of 72.0% and 80.0%, respectively. This is because the Emax and S of MT and NMT are significantly different, and the combination of the 2 can improve the ability to identify MT. The diagnostic value of Emax/D was the highest in the differentiation of PA and AL, with sensitivity and specificity of 62.3% and 82.4%, respectively. Since D was not significantly different between PA and AL, this result may suggest that in the same size of PA and AL, the maximum Young's modulus of PA is larger and the elasticity is harder.

In our study, both in the elastography group and the control group, there were statistical differences in margin, shape, architecture, posterior acoustic effect, and CDFI ($P<0.05$) between MT and NMT in conventional ultrasound, which were all included in the establishment of our classifier. Emax·S, which has the highest diagnostic value among elastography parameters, was included in the establishment of the classifier of the elastography group. In the elastography group, the AUC increased from 0.908 to 0.915, diagnostic sensitivity increased from 76% to 84%, and specificity decreased from 92.8% to 88.0% when elastic parameters were combined with conventional ultrasound. When the elastography group was compared to the control group, the AUC increased from 0.906 to 0.915, diagnostic sensitivity increased from 76% to 84%, and specificity decreased from 90.0% to 88.0%. Therefore, no matter whether in the same group of salivary gland masses, or compared with the control group, the inclusion of elastic parameters can improve the diagnostic value of salivary gland tumors and significantly improve the diagnostic sensitivity. Unfortunately, the diagnostic specificity was reduced, which seems to be the same as in Heřman *et al.*'s study. As a result, we believe that, on the basis of conventional ultrasound, the combined use of SWE still has a certain significance in the differential diagnosis of salivary gland masses.

In addition to quantitatively obtaining the Young's modulus of the mass, we also found that the color elastic map of the salivary gland mass seemed to have a certain rule. The elastography of some PAs showed a hard ring sign that the peripheral substance was red, whereas the internal substance was bluish green (*Figure 3*). This may be related to the fact that PA have a thick and tough envelope, and the tumor tends to form cracks near or along the envelope, which may lead to significant differences in the acoustic impedance inside and outside the envelope. We found that these PA tended to be small, and when the tumors were large, the elastography tended to show a disorderly interior, and the value of Young's modulus also increased correspondingly. This may be related to the fact that large PA tended to have complex pathological components that mainly included myoepithelial cells, myxoid substances, and chondroid tissues (21). As with other malignant tumors, malignant PAs often lack such signs, and are frequently characterized by hard and disorganized tissue both peripherally and internally, with chaotic patterns of blue, green, and red. This may be related to the complex composition of malignant tumors and their tendency to break through the envelope. This is consistent with Klintworth *et al.*'s suggestion (22) that the wreath sign is important for the diagnosis of MT. It is worth mentioning that in some malignant PA, despite the internal disorder, there will still be a hard ring around the perimeter, which may be caused by local malignant change of PA (*Figures 4*,*5*). The elastography of AL often shows uniform hardening without an obvious ring sign, and is heterogeneous if cystic or necrotic lesions are present internally (*Figure 6*). According to an article by Corvino *et al.* (23), B-mode ultrasound features of oncocytoma overlap with those of PA, which appears as an ovoid, well-defined, sometimes lobulated, and homogeneously hypoechoic mass. SWE may be helpful to distinguish between them, confirmation of which requires further studies due to the limited sample size.

This study also encountered some problems. Similar to conventional ultrasound, SWE attenuated to a certain extent in tissues. Deeper tumors were often not satisfactorily filled in the elastography, which affected the accurate measurement of Young's modulus (24). Therefore, in this study, masses with a depth greater than 3 cm were removed. Also, shear waves do not travel in pure fluid, so we did not include a cystic mass. If the tumor becomes liquefied and necrotic, the elastic value of the whole tumor will be inevitably affected. SWE is more objective compared with strain-elastic ultrasound that does not require additional pressure, but relies on the acoustic pulse radiation force emitted by the probe. However, it is necessary to avoid tissue pressure as far as possible in the operation process.

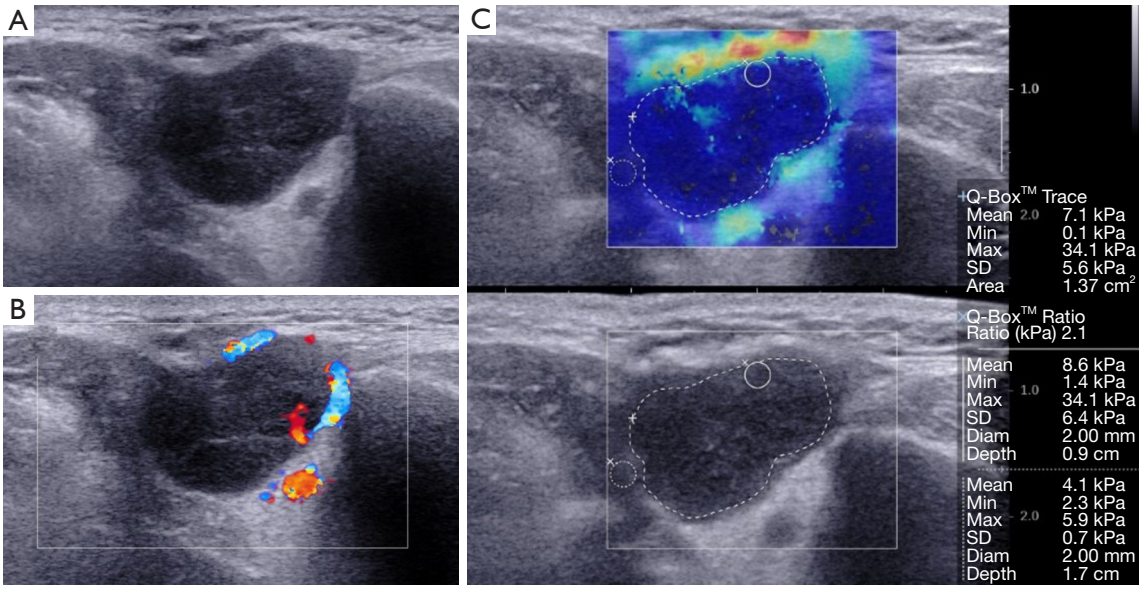

Figure 3 PA in the right parotid gland, F, 44Y. (A) B-mode ultrasound (B) CDFI: Grade 2 (C) SWE: Emax =34.1 KPa, Emean =7.1 KPa, SD =5.6 KPa, Eratio =2.1. Elastography showed stiff ring sign. PA, pleomorphic adenoma; F, female; Y, years; Emax, maximum Young's modulus; Emean, mean Young's modulus; SD, Young's modulus standard deviation; Eratio, Young's modulus ratio of mass-to-surrounding normal glands; Area, maximum cross-sectional area; Diam, size of Q-box; Depth, depth of mass; SWE, shear wave elastography.

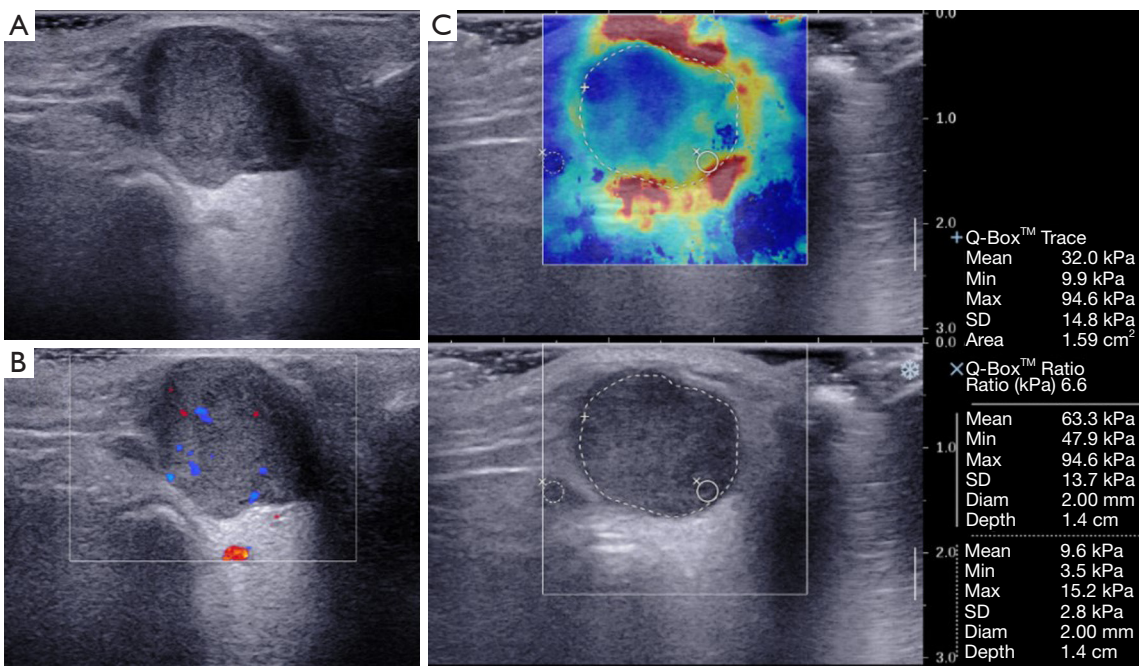

Figure 4 MPA in the left parotid gland, M, 35Y. (A) B-mode ultrasound (B) CDFI: Grade 2 (C) SWE: Emax =94.6 KPa, Emean =32.0 KPa, SD =14.8 KPa, Eratio =6.6. Elastography showed stiff ring sign with increased stiffness. MPA, malignant pleomorphic adenoma; M, male; Y, years; Emax, maximum Young's modulus; Emean, mean Young's modulus; SD, Young's modulus standard deviation; Eratio, Young's modulus ratio of mass-to-surrounding normal glands; Area, maximum cross-sectional area; Diam, size of Q-box; Depth, depth of mass; SWE, shear wave elastography.

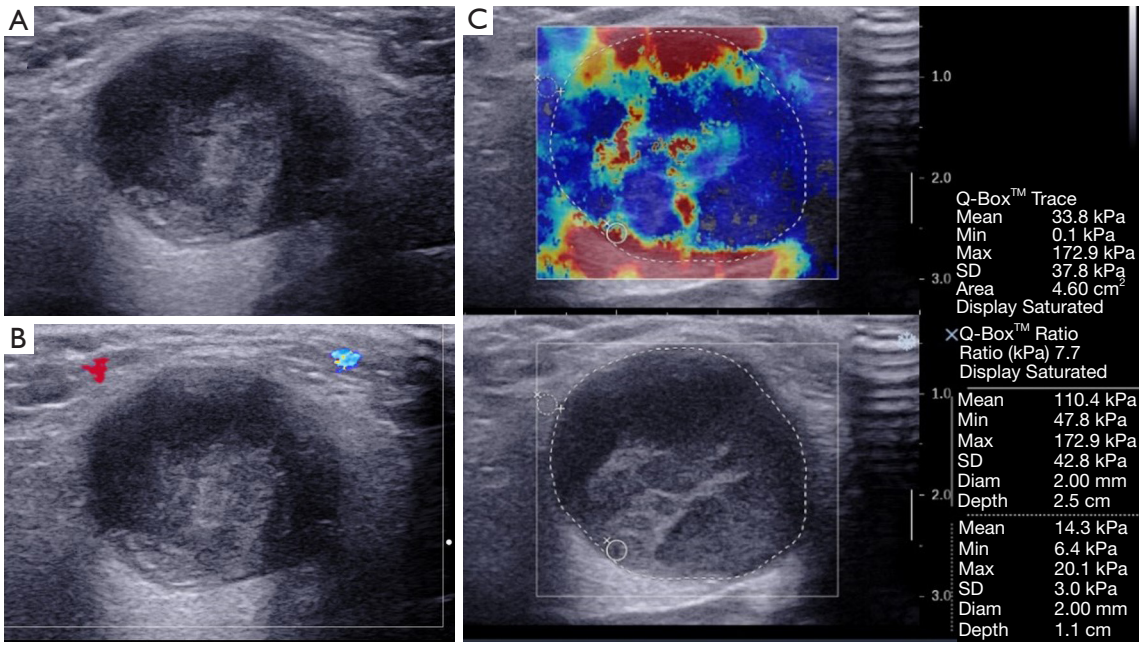

Figure 5 ACC in the right submandibular gland, F, 53Y. (A) B-mode ultrasound (B) CDFI: Grade 0 (C) SWE: Emax =172.9 KPa, Emean =33.8 KPa, SD =37.8 KPa, Eratio =7.7. Elastography showed disordered color. ACC, adenoid cystic carcinoma; M, male; Y, years; Emax, maximum Young's modulus; Emean, mean Young's modulus; SD, Young's modulus standard deviation; Eratio, Young's modulus ratio of mass-to-surrounding normal glands; Area, maximum cross-sectional area; Diam, size of Q-box; Depth, depth of mass; SWE, shear wave elastography.

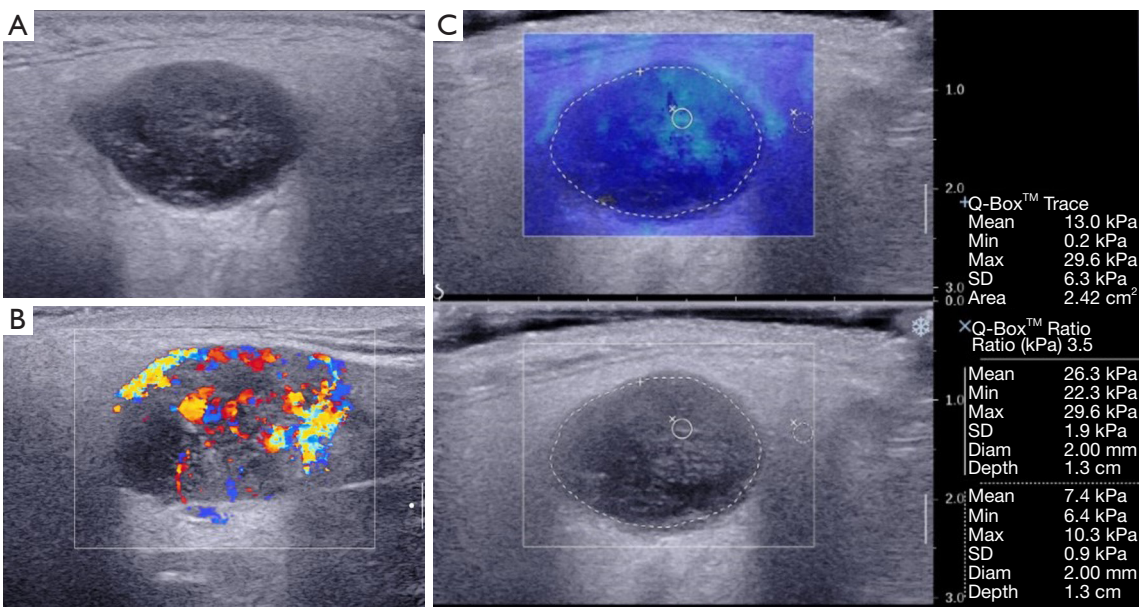

Figure 6 AL in the right parotid gland, M, 64Y. (A) B-mode ultrasound (B) CDFI: Grade 3 (C) SWE: Emax =29.6 KPa, Emean =13.0 KPa, SD =6.3 KPa, Eratio =3.5. Elastography showed homogeneous hardening. AL, adenolymphoma; M, male; Y, years; Emax, maximum Young's modulus; Emean, mean Young's modulus; SD, Young's modulus standard deviation; Eratio, Young's modulus ratio of mass-to-surrounding normal glands; Area, maximum cross-sectional area; Diam, size of Q-box; Depth, depth of mass; SWE, shear wave elastography.

The salivary glands are located in the head and neck and their soft tissue is thinner, so a salivary gland tumor is more likely to protrude from the surface. In this instance, we thickly applied ultrasound gel to increase the buffering effect. In our study, the uniform blue color on the elastic map of the surface soft tissue of the mass was taken as the quality control standard to minimize the influence of manipulation.

Conclusions

As a new ultrasonic diagnostic technique, SWE can be used as a supplemental method for the diagnosis of salivary gland tumors, which has certain value in improving the diagnostic sensitivity of MT, and the differential diagnosis of PA and AL. It has a certain significance for clinicians in the development of treatment plans for salivary gland tumors.

Acknowledgments

Funding: This work was supported by the National Natural Science Foundation of China (No. 81971618), the Shanghai Municipal Commission of Science and Technology (No. 23ZR1438000), and the Ninth People's Hospital, Shanghai Jiaotong University School of Medicine (No. JYJC202132).

Footnote

Reporting Checklist: The authors have completed the STARD reporting checklist. Available at https://qims.amegroups.com/article/view/10.21037/qims-23-103/rc

Conflicts of Interest: All authors have completed the ICMJE uniform disclosure form (available at https://qims.amegroups.com/article/view/10.21037/qims-23-103/coif). All authors report this work was supported by the National Natural Science Foundation of China (No. 81971618), the Shanghai Municipal Commission of Science and Technology (No. 23ZR1438000), and the Ninth People's Hospital, Shanghai Jiaotong University School of Medicine (No. JYJC202132). The authors have no other conflicts of interest to declare.

Ethical Statement: The authors are accountable for all aspects of the work in ensuring that questions related to the accuracy or integrity of any part of the work are appropriately investigated and resolved. The study was conducted in accordance with the Declaration of Helsinki (as revised in 2013). The study was approved by the Ethics Committee of the Ninth People's Hospital, Shanghai Jiaotong University School of Medicine and individual consent for this retrospective analysis was waived.

References

1. Carlson ER, Schlieve T. Salivary Gland Malignancies. Oral Maxillofac Surg Clin North Am 2019;31:125-44.
2. Guzzo M, Locati LD, Prott FJ, Gatta G, McGurk M, Licitra L. Major and minor salivary gland tumors. Crit Rev Oncol Hematol 2010;74:134-48.
3. Li C, Zhang C, Li N, Li J. Compression Real-time Elastography for Evaluation of Salivary Gland Lesions: A Meta-analysis. J Ultrasound Med 2016;35:999-1007.
4. Christe A, Waldherr C, Hallett R, Zbaeren P, Thoeny H. MR imaging of parotid tumors: typical lesion characteristics in MR imaging improve discrimination between benign and malignant disease. AJNR Am J Neuroradiol 2011;32:1202-7.
5. Stanek JJ, Khariwala SS. What Is the Utility of Fine-Needle Aspiration in Parotid Gland Neoplasms? Laryngoscope 2019;129:1255-6.
6. Skálová A, Hyrcza MD, Leivo I. Update from the 5th Edition of the World Health Organization Classification of Head and Neck Tumors: Salivary Glands. Head Neck Pathol 2022;16:40-53.
7. Matsuda E, Fukuhara T, Donishi R, Kawamoto K, Hirooka Y, Takeuchi H. Usefulness of a Novel Ultrasonographic Classification Based on Anechoic Area Patterns for Differentiating Warthin Tumors from Pleomorphic Adenomas of the Parotid Gland. Yonago Acta Med 2017;60:220-6.
8. Sacks D, Baxter B, Campbell BCV, Carpenter JS, Cognard C, et al. Multisociety Consensus Quality Improvement Revised Consensus Statement for Endovascular Therapy of Acute Ischemic Stroke. Int J Stroke 2018;13:612-32.
9. Riegler J, Labyed Y, Rosenzweig S, Javinal V, Castiglioni A,

Dominguez CX, Long JE, Li Q, Sandoval W, Junttila MR, Turley SJ, Schartner J, Carano RAD. Tumor Elastography and Its Association with Collagen and the Tumor Microenvironment. Clin Cancer Res 2018;24:4455-67.
10. Chen X, Wang L, Li X, Fu P, Xu M, Zou C, Li X, Dong Y. Can virtual touch tissue imaging quantification be a reliable method to detect anterior talofibular ligament type I injury at the acute, subacute, and chronic stages? Quant Imaging Med Surg 2021;11:4334-41.
11. Bamber JC. Ultrasound elasticity imaging: definition and technology. Eur Radiol 1999;9 Suppl 3:S327-30.
12. Shiina T, Nightingale KR, Palmeri ML, Hall TJ, Bamber JC, Barr RG, et al. WFUMB guidelines and recommendations for clinical use of ultrasound elastography: Part 1: basic principles and terminology. Ultrasound Med Biol 2015;41:1126-47.
13. Gu J, Polley EC, Denis M, Carter JM, Pruthi S, Gregory AV, Boughey JC, Fazzio RT, Fatemi M, Alizad A. Early assessment of shear wave elastography parameters foresees the response to neoadjuvant chemotherapy in patients with invasive breast cancer. Breast Cancer Res 2021;23:52.
14. Cassinotto C, Boursier J, Paisant A, Guiu B, Irles-Depe M, Canivet C, Aube C, de Ledinghen V. Transient Versus Two-Dimensional Shear-Wave Elastography in a Multistep Strategy to Detect Advanced Fibrosis in NAFLD. Hepatology 2021;73:2196-205.
15. Mansour N, Bas M, Stock KF, Strassen U, Hofauer B, Knopf A. Multimodal Ultrasonographic Pathway of Parotid Gland Lesions. Ultraschall Med 2017;38:166-73.
16. Bhatia KS, Cho CC, Tong CS, Lee YY, Yuen EH, Ahuja AT. Shear wave elastography of focal salivary gland lesions: preliminary experience in a routine head and neck US clinic. Eur Radiol 2012;22:957-65.
17. Wierzbicka M, Kałużny J, Szczepanek-Parulska E, Stangierski A, Gurgul E, Kopeć T, Ruchała M. Is sonoelastography a helpful method for evaluation of parotid tumors? Eur Arch Otorhinolaryngol 2013;270:2101-7.
18. Cantisani V, David E, Sidhu PS, Sacconi B, Greco A, Pandolfi F, Tombolini M, Lo Mele L, Calliada F, Brunese L, Catalano C, De Vincentiis M, Di Leo N, Ascenti G, D'Ambrosio F. Parotid Gland Lesions: Multiparametric Ultrasound and MRI Features. Ultraschall Med 2016;37:454-71.
19. Evans A, Whelehan P, Thomson K, Brauer K, Jordan L, Purdie C, McLean D, Baker L, Vinnicombe S, Thompson A. Differentiating benign from malignant solid breast masses: value of shear wave elastography according to lesion stiffness combined with greyscale ultrasound according to BI-RADS classification. Br J Cancer 2012;107:224-9.
20. Heřman J, Sedláčková Z, Vachutka J, Fürst T, Salzman R, Vomáčka J, Heřman M. Differential Diagnosis of Parotid Gland Tumors: Role of Shear Wave Elastography. Biomed Res Int 2017;2017:9234672.
21. Olgun DC, Kantarci F, Taskin U, Kilic F, Oktay MF, Altinay S, Kepil N, Adaletli I, Ada M, Mihmanli I. Relative proportions of stromal to cellular components of pleomorphic adenomas: determination with shear wave elastography. J Ultrasound Med 2014;33:503-8.
22. Klintworth N, Mantsopoulos K, Zenk J, Psychogios G, Iro H, Bozzato A. Sonoelastography of parotid gland tumours: initial experience and identification of characteristic patterns. Eur Radiol 2012;22:947-56.
23. Corvino A, Caruso M, Varelli C, Di Gennaro F, Pignata S, Corvino F, Vallone G, Catalano O. Diagnostic imaging of parotid gland oncocytoma: a pictorial review with emphasis on ultrasound assessment. J Ultrasound 2021;24:241-7.
24. Chou SS, Baikpour M, Zhang W, Mercaldo SF, Lehman CD, Samir AE. Shear-Wave Elastography of the Breast: Impact of Technical Image Quality Parameters on Diagnostic Accuracy. AJR Am J Roentgenol 2021;216:1205-15.

Cite this article as: Yu Q, Ding A, Chen Q, Zuo J, Cao J, Xiong P. Diagnostic value of shear wave elastography quantification combined with conventional ultrasound in salivary gland tumors. Quant Imaging Med Surg 2023;13(9):5863-5876. doi: 10.21037/qims-23-103

